

Probing Dark Matter annihilation in the Galactic Centre with TRIDENT

Yingwei Wang^{*,a}, Xinhui Chu^{*,a}, Andrew Cheek^{,a,b},
 Iwan Morton-Blake^{**,a}, Qichao Chang^a, Gwenael Giacinti^a, Samy
 Kaci^a, Xin Xiang^{**,a,b,c}, Donglian Xu^{a,b,c} and Fuyudi Zhang^a**

^aState Key Laboratory of Dark Matter Physics, Tsung-Dao Lee Institute & School of Physics and Astronomy, Shanghai Jiao Tong University, Shanghai 200240, China

^bKey Laboratory for Particle Astrophysics and Cosmology (MOE) & Shanghai Key Laboratory for Particle Physics and Cosmology, Shanghai Jiao Tong University, Shanghai 200240, China

^cHainan Research Institute, Shanghai Jiao Tong University, Hainan 572024, China

E-mail: yingweiw@sjtu.edu.cn, sjtu3915211@sjtu.edu.cn, acheek@sjtu.edu.cn,
iblake@sjtu.edu.cn, xxiang@sjtu.edu.cn

Abstract. We determine the future sensitivity of the TRIDENT neutrino telescope to dark matter annihilation in the Galactic Centre. By applying the full detector design we show that TRIDENT will probe annihilation rates down to $\langle\sigma v\rangle \approx 5 \times 10^{-27} \text{ cm}^3 \text{ s}^{-1}$ for a 10 TeV dark matter, which is below the thermal freeze-out benchmark. The analysis is carried out with all-flavour neutrino interactions, where we demonstrate that cascade events, primarily due to $\nu_{e,\tau}$, show greater sensitivity to a dark matter signal compared to the more commonly studied track events. Furthermore, we highlight the impact of a previously overlooked background, Galactic neutrinos produced from interactions between hadronic cosmic rays and interstellar gas. We find dark matter sensitivities are more strongly degraded in the high energy region above ~ 10 TeV, with a maximal weakening of approximately a factor of ~ 2 . This effect remains smaller than the uncertainty associated with the dark matter density profile but can nonetheless mimic a positive annihilation signal. We contextualize these results with a concrete particle model and show that TRIDENT will be able to probe the most interesting untested parts of parameter space.

^{*}These authors contributed equally to this work.

^{**}Corresponding authors.

Contents

1	Introduction	1
2	Neutrino Flux From Dark Matter Annihilation	2
3	The TRIDENT Detector	3
3.1	Neutrino Interactions in TRIDENT	3
3.2	Simulation Framework	4
4	Model-independent Limits	4
4.1	Likelihood Construction and Background Modelling	5
4.2	Standard Sensitivity	8
4.3	Galactic Plane Neutrino Background	9
4.4	Dark Matter Halo Model	9
5	Particle Model Inference and Complementarity	11
5.1	The $L_i - L_j$ Model	13
6	Summary and Outlook	15

1 Introduction

Unveiling the nature of dark matter (DM) remains a fundamental challenge in modern physics [1, 2]. Thermal freeze-out of heavy stable particles [3, 4] provides an elegant production mechanism for DM in the early Universe while necessitating new interactions with the Standard Model (SM). This process is driven by the thermally averaged DM annihilation cross-section, $\langle\sigma v\rangle$. What is more, for a large range of DM masses, $0.1 - 10^5$ GeV, the cross-section required to produce the correct relic varies very little $\langle\sigma v\rangle \approx 3 \times 10^{-26} \text{ cm}^3 \text{ s}^{-1}$ [5, 6]. Annihilation with such a cross-section should in principle be observable in regions of high DM density, motivating experimental searches. This method of *indirect detection* [7–9] has made substantial progress in the last decades, with the most successful experiments using photons and anti-particles as messengers [10–13]. However, the thermal freeze-out target above ~ 100 GeV remains largely untested [14]. At such high energies, while γ -ray telescopes have shown steady progress [15–18], neutrino telescopes have emerged as excellent astrophysical tools [19–22]. In this work we assess the future capabilities of the TRopIcal DEep-sea Neutrino Telescope (TRIDENT) precisely in the search for DM in the $10^3 - 10^5$ GeV mass range.

TRIDENT is a next-generation neutrino observatory in the South China Sea. Advanced photosensitive detectors occupying a multi-cubic kilometre volume of seawater which would constitute the largest fiducial volume for an underwater neutrino telescope. Unlike other next-generation neutrino telescopes, such as IceCube-Gen2, which operates in Antarctic ice for TeV-scale neutrinos [21], and KM3NeT, deployed in Mediterranean waters [22], TRIDENT’s seawater-based design optimises all-flavour neutrino detection, particularly high-energy cascade events. This paper presents the first model-independent sensitivity projections for TRIDENT’s DM annihilation search. We target the Galactic Centre, demonstrating

TRIDENT’s potential for reaching cross-sections consistent with the DM thermal freeze-out benchmark. These projections guide pre-deployment detector optimisations and establish the analysis framework for future DM searches, positioning TRIDENT as a leading probe of the high-mass DM parameter space.

An additional novel feature of this article is our treatment of the Galactic plane neutrinos, which are produced from interactions between hadronic cosmic rays and interstellar gas. Such a background can significantly affect DM searches in the Galactic Centre and has not been included in previous studies [23]. We adopt the Galactic plane neutrino flux inferred from the IceCube observations [24] and quantitatively evaluate its impact on the TRIDENT sensitivity.

In this article, we first review the basics for determining the neutrino flux from DM annihilation in the centre of the Galaxy in Section 2. In Section 3, we describe the detector setup and simulation framework used to estimate the event rates for the DM signal and expected backgrounds. In Section 4 we present the TRIDENT sensitivity analysis and then evaluate the effects of the unknown Galactic neutrino background and halo profile uncertainties. In Section 5 we interpret these future projections for a specific particle physics model, exemplifying how TRIDENT will be able to uniquely probe important regions of the DM parameter space, and potentially discover it. Finally we summarise our findings and discuss future directions in Section 6.

2 Neutrino Flux From Dark Matter Annihilation

For neutrino telescopes, the neutrino flux from DM annihilation is

$$\frac{d\Phi_\nu}{dE_\nu} = \frac{1}{4\pi} \frac{\langle\sigma v\rangle}{\kappa m_\chi^2} \left(\sum_\alpha \frac{dN_{\nu\alpha}^{\text{prod}}}{dE_{\nu\alpha}} P_{\nu\alpha \rightarrow \nu\beta} \right) J(\Omega) \quad (2.1)$$

where m_χ is the DM mass and $dN_\nu^{\text{prod}}/dE_\nu$ is the neutrino energy spectrum per annihilation, the superscript ‘prod’ signifies that this spectrum is calculated at the production point. For the $\nu\bar{\nu}$ final state the energy spectrum is simply a neutrino line, $dN_\nu/dE = 2\delta(E_\nu - m_\chi)$, for 4ν final states the energy spectrum is box-shaped, $dN_\nu/dE = 4H(m_\chi - E_\nu)/m_\chi$, where H is the Heaviside step function [25, 26]. For non-neutrino final states, such as quarks and charged leptons, neutrinos are still radiated from showering and particle decay, generating a continuous spectrum. We use the spectra provided in the code χarov [27]¹. The propagation from the source to detection is encapsulated by the transition probability $P_{\nu\alpha \rightarrow \nu\beta}$. To calculate this, we take the best-fit PMNS matrix values from Ref. [30]. The numerical factor κ is determined by the nature of DM. In the case of self-conjugate particles (such as Majorana fermions or real scalars), $\kappa = 2$, whereas for non-self-conjugate particles (such as Dirac fermions or complex scalars), $\kappa = 4$. We adopt $\kappa = 2$ for our model-independent analysis. Finally, $J(\Omega)$ in Eq. (2.1) is the integral of the DM density ρ_χ along the line of sight dx (l.o.s.) over the target solid angle in the sky $d\Omega$, namely the J-factor

$$J \equiv \int d\Omega \int_{\text{l.o.s.}} \rho_\chi^2(x) dx. \quad (2.2)$$

The precise form of the DM density profile is one of the main sources of uncertainty for our signal. For our model-independent bounds we will consider the benchmark NFW

¹Note that we have checked our results are consistent when using other codes such as HDMSpectra [28] and CosmiXs [29].

profile [31]

$$\rho_\chi(r) = \frac{\rho_s}{(r/r_s)(1+r/r_s)^2} \quad (2.3)$$

where $r_s = 20$ kpc is the scale radius and ρ_s is the scale density, which is fixed by a local DM density $\rho_0 = 0.4$ GeV cm⁻³ [32]. For each direction in the sky, we calculate the J-factor and use this as the spatial template for the DM signal. We discuss the dependence of our results with respect to the density profile choices in Section 4.4.

3 The TRIDENT Detector

TRIDENT is a planned next-generation deep-sea neutrino telescope to be constructed in the South China Sea, at a depth of approximately 3.5 km. The full detector will comprise up to ~ 1000 vertical strings, spanning several cubic kilometres, each instrumented with hybrid Digital Optical Modules (hDOMs) [33].

3.1 Neutrino Interactions in TRIDENT

The TRIDENT detector is designed to achieve full-sky coverage and detect with a high efficiency for all neutrino flavours over a broad energy range, from sub-TeV to multi-PeV. Long optical scattering lengths in deep seawater allow for excellent photon timing and spatial resolution, boosting precision in the reconstruction of neutrino directions. These features make TRIDENT particularly well-suited for studying extended and diffuse astrophysical sources such as the Galactic Centre and for searching for DM annihilation signals.

Neutrino interactions in large-scale Cherenkov detectors such as TRIDENT produce two main event topologies: track and cascade-like events (referenced as tracks and cascades later in this work, respectively), corresponding to different neutrino flavours and interaction types.

Tracks arise primarily from charged-current (CC) interactions of ν_μ , producing energetic muons that may traverse several kilometres in water. Their elongated light pattern enables precise directional reconstruction and provides the basis for point-source searches. The dominant background for these events comes from atmospheric muons generated by cosmic-ray interactions, which overwhelm the down-going event rate below ~ 100 TeV. Consequently, TRIDENT’s searches for astrophysical ν_μ signals focus on up-going tracks.

Cascades originate from CC interactions of ν_e and ν_τ , as well as neutral-current (NC) interactions of all flavours. They deposit energy within a more confined region (on the order of metres) compared to tracks, yielding a more limited angular resolution. However, for spatially extended or diffuse sources, such as the Galactic Centre, precise directionality is less critical, making cascades an important signal channel. Cascades also provide superior energy resolution, since their energy is typically fully contained within the detector, and suffer less contamination from atmospheric muons and neutrinos. Together with full-sky coverage and flavour inclusivity, these features make cascades an essential complement to tracks in DM searches. This study therefore considers both channels in combination, ensuring sensitivity to all neutrino flavours and interaction types.

Example track and cascade events simulated using TRIDENT’s simulation framework, described in the following section, are shown in Fig. 1, highlighting the significant differences in energy deposition possible for each interaction type within the detector.

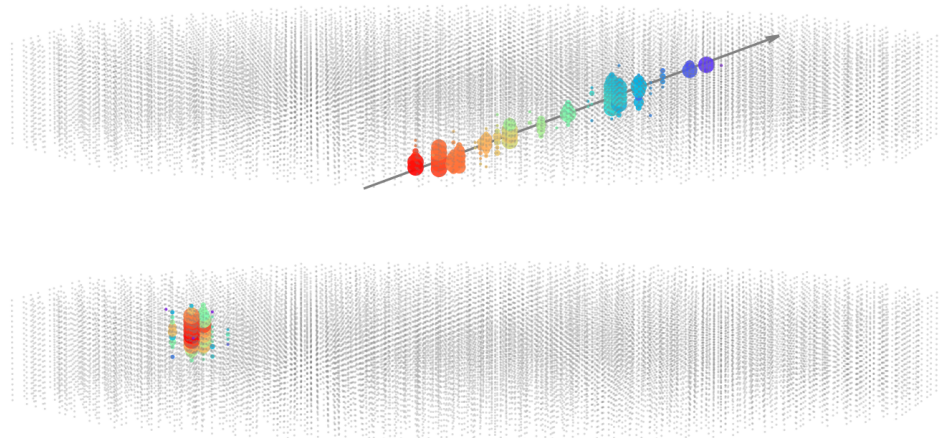


Figure 1: Visualisation of the two types of neutrino interactions from the TRIDENTSim framework [34], showing an example ν_μ -CC track event (top) and ν_e -CC cascade event (bottom). The colour of the spheres indicates the photon detection time, with red corresponding to early arrivals and blue to later arrivals, while the radii represent the number of photons detected by each hDOM.

3.2 Simulation Framework

The detector response and sensitivity estimates presented in this work are based on the TRIDENTSim full-chain Monte Carlo framework [34]. The simulation models neutrino interactions of all flavours, including propagation through the Earth, deep inelastic scattering near the detector, and the subsequent production and propagation of secondary particles using PYTHIA8 [35], CRMC [36], and GEANT4 [37]. Cherenkov photon production and propagation are simulated with GEANT4 and the OPTIX ray-tracing engine [38], incorporating the measured optical properties of seawater at the TRIDENT site [39]. The reconstruction of key neutrino direction and energy parameters is carried out using dedicated track and cascade likelihood-based algorithms [34]. These define the effective areas and angular resolutions used in the DM sensitivity calculations presented in the following sections.

4 Model-independent Limits

In this section, we present the projected sensitivities of TRIDENT to DM annihilation into SM particles. The analysis follows a maximum-likelihood approach, applied separately to track and cascade neutrino event channels.

We first describe the likelihood construction and statistical treatment, then show the resulting model-independent limits under standard assumptions for the atmospheric and astrophysical neutrino backgrounds. Finally, we assess the impact of an additional Galactic neutrino component from cosmic-ray interactions, and discuss systematic uncertainties related to the DM halo model.

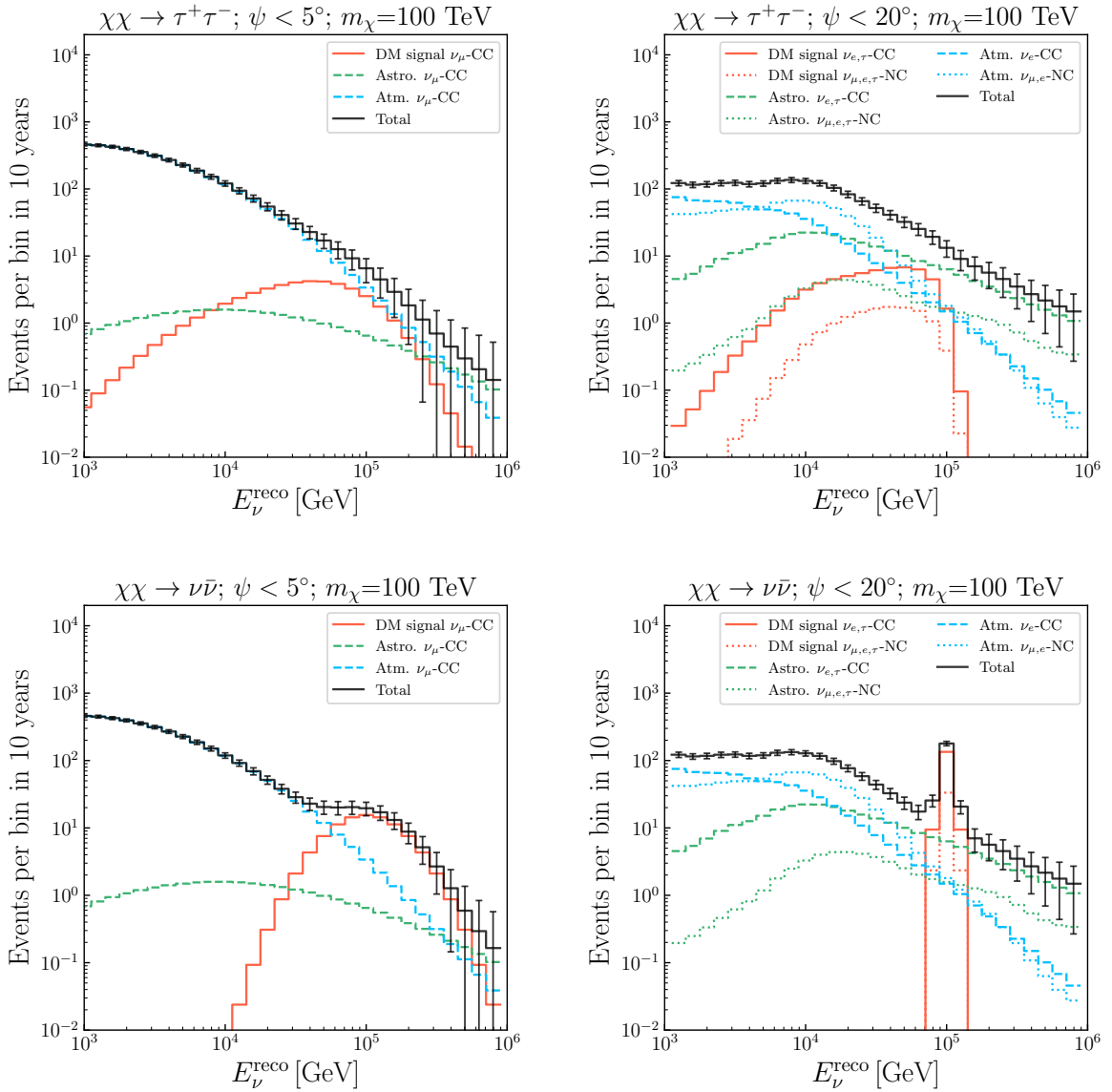


Figure 2: Expected reconstructed energy spectra in TRIDENT from DM annihilation channels $\chi\chi \rightarrow \tau^+\tau^-$ (top) and $\chi\chi \rightarrow \nu\bar{\nu}$ (bottom) for a DM mass of $m_\chi = 100$ TeV. The left and right panels correspond to track events with opening angle $\psi < 5^\circ$ and cascade events with $\psi < 20^\circ$, respectively. The annihilation cross-section $\langle\sigma v\rangle$ is adopted from the current KM3NeT limits [40]. The smeared distributions account for the detector's energy reconstruction uncertainty.

4.1 Likelihood Construction and Background Modelling

We evaluate TRIDENT's sensitivity to DM annihilation signals using the track and cascade channels separately. DM signal events are extracted through the reconstructed sky map distribution of neutrino events in the Galactic Centre, where the angular resolution performance for both track and cascade events can be seen in Ref. [34]. Similarly described in this work,

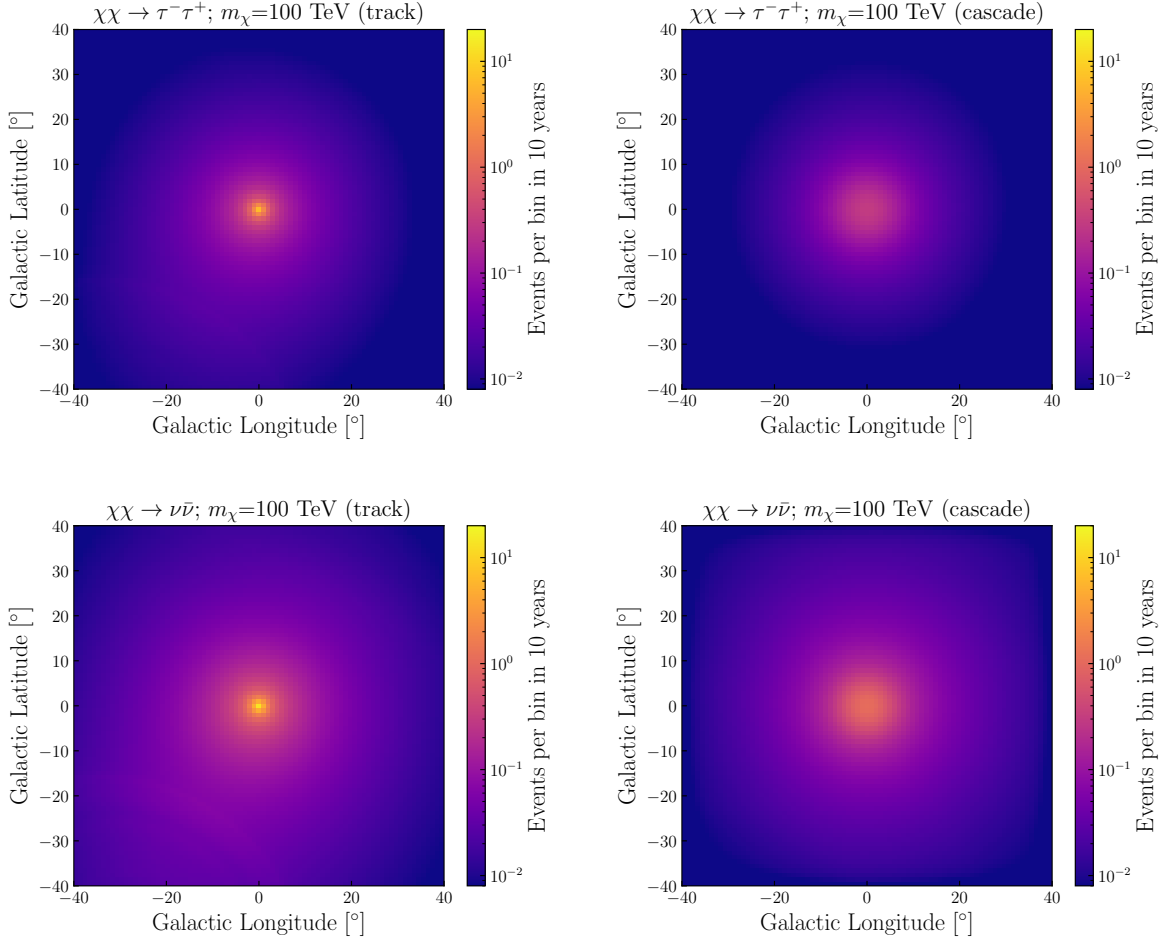


Figure 3: Reconstructed sky maps of expected DM signals in TRIDENT in Galactic coordinates, extending $\pm 40^\circ$ in both latitude and longitude. The signals arise from DM annihilation channels $\chi\chi \rightarrow \tau^+\tau^-$ and $\chi\chi \rightarrow \nu\bar{\nu}$ for a DM mass of $m_\chi = 100$ TeV. The annihilation cross-section $\langle\sigma v\rangle$ is taken from the current KM3NeT limits [40]. The distributions account for the detector’s angular resolution.

signal and background event rates are determined using TRIDENT’s calculated effective area, which implements a detector-level trigger based on a minimum number of hDOMs with co-incident photons detected. Basic analysis cuts are similarly applied. For track events only reconstructed *up-going* events ($\theta_z > 90^\circ$) are considered in order to suppress the large background from atmospheric muons. Cascade events conversely are selected from *all directions*, as the diffuse nature of Galactic sources reduces dependence on strict angular cuts.

To account for energy reconstruction resolutions, a Gaussian smearing approximation is assumed based on preliminary energy reconstruction methods developed for the TRIDENT detector, applying: $\Delta \log_{10}(E_{\text{reco}}/E_\nu) = 0.25$ for tracks and 0.04 for cascades, corresponding to energy resolution of $\sim 80\%$ and $\sim 10\%$, respectively.

The expected event counts, μ , for an effective exposure time T are computed as a convolution of the declination-dependent effective area $A_{\text{eff}}(E_\nu, \delta)$ and the neutrino intensity

$$d\Phi_\nu/dE_\nu$$

$$\mu = T \int d\Omega \int dE_\nu \frac{d\Phi_\nu}{dE_\nu} A_{\text{eff}}(E_\nu, \delta), \quad (4.1)$$

The total expected event rate includes both **signal** and **background** components. The dominant backgrounds are:

- **Atmospheric neutrinos**, modelled using the `DaemonFlux` package [41], including both conventional and prompt components.
- **Atmospheric muons**, are assumed to be effectively removed through an up-going reconstructed directional cut, applied to track events only.
- **Diffuse astrophysical neutrinos**, modelled as an isotropic flux following IceCube’s best-fit power law [42].
- **Galactic plane neutrinos**, measured by the IceCube experiment [24], are expected to be a measurable background for potential DM signal neutrinos produced in the same region. Further discussions on this background and its expected impact are found in Section 4.3

The estimation of TRIDENT sensitivities on the upper limits of the thermally averaged DM annihilation cross-section $\langle\sigma v\rangle$ is performed using the maximum-likelihood method. The likelihood function \mathcal{L} is defined as

$$\mathcal{L}(\langle\sigma v\rangle) = \prod_{ij} \frac{(s_{ij} + b_{ij})^{n_{ij}}}{n_{ij}!} e^{-(s_{ij} + b_{ij})}, \quad (4.2)$$

where s_{ij} and b_{ij} are the expected signal and background events in the i th energy bin and j th angular bin, and n_{ij} is the observed count (background-only in sensitivity studies).

The expected DM signal and background reconstructed neutrino energies for a 10-year exposure are shown in Fig. 2 and Fig. 3. The event rate of the signals and background decomposed into individual interaction components is presented in Fig. 2 as a function of neutrino energy, assuming maximum opening angles of $\psi = 5^\circ$ for track events and $\psi = 20^\circ$ for cascade events, while Fig. 3 displays the corresponding sky map of the DM signals obtained with $\psi = 40^\circ$. The neutrino spectra are calculated for DM annihilation channels $\chi\chi \rightarrow \tau^+\tau^-$ and $\chi\chi \rightarrow \nu\bar{\nu}$ with a DM mass of 100 TeV, adopting the annihilation cross-section $\langle\sigma v\rangle$ constrained by current KM3NeT limits [40].

The sensitivity for each annihilation channel hypothesis is evaluated through the fits of Asimov datasets using the test statistic, which is defined by the ratio of the maximized likelihood and the null hypothesis likelihood [43]

$$\text{TS} = -2 \ln \left(\frac{\mathcal{L}(\hat{s})}{\mathcal{L}(s=0)} \right). \quad (4.3)$$

The value of cross-section $\langle\sigma v\rangle$ that yields a number of signal events \hat{s} corresponding to the 95% confidence level criterion is taken as the upper limit.

4.2 Standard Sensitivity

We forecast the sensitivity of TRIDENT to DM annihilation into some specific SM final states, assuming a 100% branching ratio for each channel.

In Fig. 4 we show the 95% CL upper limits for the $b\bar{b}$, $\tau^+\tau^-$, $\nu\bar{\nu}$ and 4ν channels obtained from the maximum-likelihood analysis. The lines represent the median expected limits, while the colour bands denote the 68% intervals around the expected value, taking into account the statistical uncertainties from Monte Carlo simulations. The sensitivity derived from track events is shown in the left plot, whereas the right plot depicts the sensitivity obtained from cascade events.

Overall, the limits exhibit a clear hierarchy among the annihilation channels. The $b\bar{b}$ and $\tau^+\tau^-$ final states yield comparatively weaker sensitivities, primarily because these channels produce broader secondary particles and softer neutrino spectra. The neutrino-direct channels ($\nu\bar{\nu}$ and 4ν) provide the strongest sensitivities as expected, since annihilation directly into neutrinos produces a sharply peaked and hard neutrino spectrum. Both analyses based on tracks and cascades are expected to reach the thermal relic value around multi-TeV for $\nu\bar{\nu}$ and 4ν channels. The sensitivities of cascades benefit from the better energy resolution, which provides a boost for all the channels. The relative behaviour of the 4ν and $\nu\bar{\nu}$ channels diverges between the two event topologies. For tracks, the limits for 4ν nearly overlap with those of $\nu\bar{\nu}$, since track events have relatively poor energy resolution and are thus less sensitive to the differences in the injected neutrino spectrum, leading to comparable sensitivities. In contrast, the more precise energy reconstruction of cascades makes the spectra from box-shaped 4ν flux and line-like $\nu\bar{\nu}$ flux distinguishable. As a result, the cascade channel achieves better sensitivities for the $\nu\bar{\nu}$ channel against the 4ν channel.

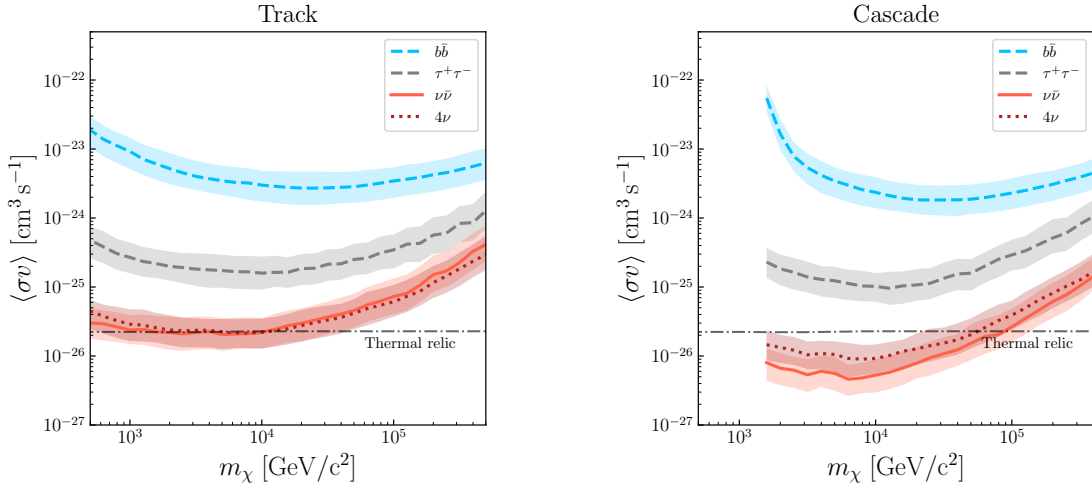


Figure 4: 95% CL upper limits of TRIDENT on the thermally averaged DM annihilation cross-section $\langle\sigma v\rangle$, as a function of the DM mass for four annihilation channels. The left (right) panel represents the sensitivity obtained from track (cascade) events.

4.3 Galactic Plane Neutrino Background

In addition to the previously considered atmospheric and diffuse astrophysical neutrinos, Galactic neutrino emission originating from the interactions of hadronic cosmic rays with interstellar gas is also expected [24]. To describe this additional neutrino background, we follow the modelling of Refs. [44–46], where cosmic rays are injected by individual sources with a discrete distribution of positions.

Galactic neutrinos contribute in the form of two components, diffuse Galactic neutrino emission and Galactic neutrino source emission. The former is concentrated on the Galactic plane, roughly following the distribution of interstellar gas up to a few tens of TeV (taken from Refs. [47, 48] for this work), while for higher energies, discrepancies between the gas and neutrino distributions begin to appear due to stochastic effects [44]. The latter component is derived from the contribution of individual sources due to the presence of a local cosmic-ray injector.

As a result, this contribution is stochastic by nature and depends on the unknown positions of neutrino sources in the Galaxy. This approach is more physically motivated than the use of propagation codes, such as GALPROP [49] and DRAGON [50, 51], which assume a smooth distribution of cosmic-ray sources in the Galaxy. The shorter confinement time of TeV – PeV cosmic rays, compared to GeV counterparts, leads to more visible imprints from individual sources. TRIDENT sensitivities to DM should also be reevaluated without prior knowledge of the expected distribution of the Galactic neutrinos.

To overcome this difficulty, we applied the following procedure. First, we randomly generate different realizations of our Galaxy, where the Galactic neutrino emission is generated by a different set of Galactic sources drawn randomly for each simulation. This gives different sky maps of the Galactic neutrino flux. Fig. 5 shows the event rate obtained using one such randomly generated Galactic plane sky map, together with the DM signal from $\chi\chi \rightarrow \nu\bar{\nu}$ channel and the atmospheric combined with diffuse astrophysical background contributions. Following this, some maps are randomly selected to form Asimov datasets of the potential DM signal, while others are used as probability distribution functions in the sensitivity calculation. This process is repeated ten times for distinct pairs of sky maps, where the average sensitivity was taken. This approach is expected to account for the loss of sensitivity due to the absence of information in the distributions of the Galactic plane neutrino flux.

The result of such a procedure is shown in Fig. 6, which shows the sensitivity to DM as a function of DM mass for track (cyan) and cascade events (purple), including and excluding (solid and dashed, respectively) Galactic neutrino emission. For the track events, we see that the Galactic plane neutrino background weakens TRIDENT’s sensitivity above ~ 6 TeV whereas for cascades we see the limit is weaker even at 2 TeV, due to their worse angular resolution.

4.4 Dark Matter Halo Model

In addition to the neutrino backgrounds mentioned above, substantial uncertainties of the DM density profile can significantly limit TRIDENT’s sensitivity to $\langle\sigma v\rangle$. Efforts to understand the potential density profile primarily come from astrometry and N-body cosmological simulations. Modern N-body simulations such as Auriga L3 [52, 53], FIRE-2 [54], VINTERGATAN-GM [55], TNG50 [56], incorporate baryonic effects. Furthermore, in the era of survey telescopes such as Gaia [57–59], astrometry studies are also able to provide competitive constraints on the profile in the Milky Way [60, 61].

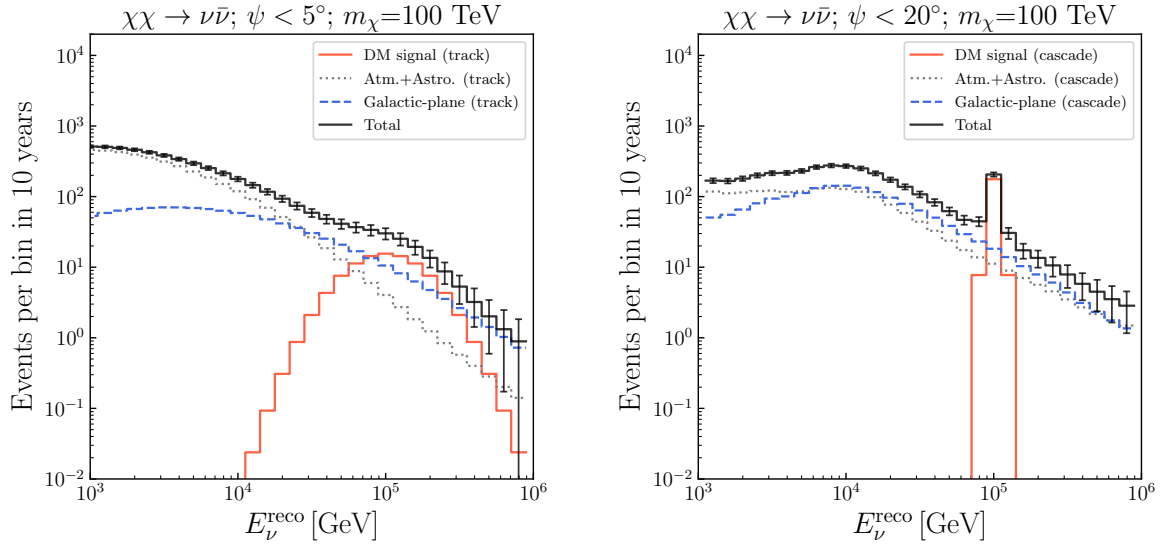


Figure 5: The event rate of Galactic plane neutrinos background from one randomly generated sky map, together with the DM signal from $\chi\chi \rightarrow \nu\bar{\nu}$ channel and the combined atmospheric and diffuse astrophysical background, for both track (left) and cascade (right) events.

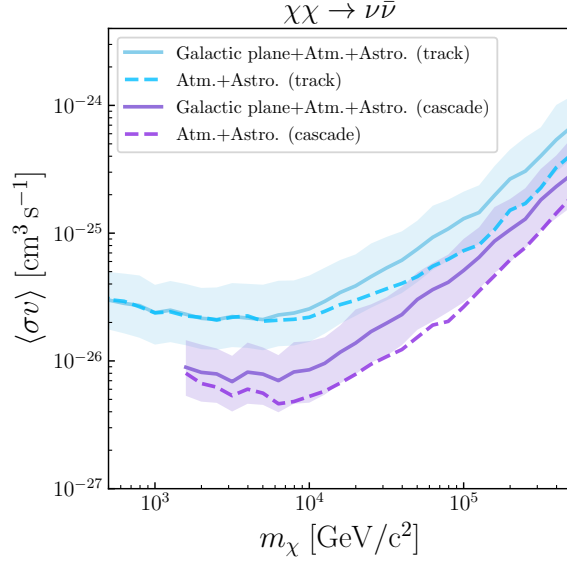


Figure 6: DM signal sensitivity of the $\chi\chi \rightarrow \nu\bar{\nu}$ channel for both track (cyan) and cascade (purple) events, shown with and without the inclusion of Galactic plane background (solid and dashed, respectively). Coloured bands represent 68% uncertainty intervals.

Despite substantial progress, the uncertainty in the profile remains large, especially in the central regions. Ref. [62] proposed using a ‘bracketed’ profile, which takes the state-of-the-art results from N-body simulations and astrometry in order to quantify our ignorance, see Fig. 2 of Ref. [62]. The profile maintains an uncertainty slightly below one order of magnitude in the

inner region ($\lesssim 1$ kpc), but it's the halo uncertainty to disfavour profiles with a large core. In Fig. 7 we show the effect this bracketed halo function has on our projected sensitivity; panels left and right show our results for track and cascade signals, respectively. We see that for both track and cascades, the TRIDENT sensitivity is affected by around an order of magnitude. The halo uncertainty, therefore, will be the leading cause of uncertainty in TRIDENT's sensitivity to DM annihilations.

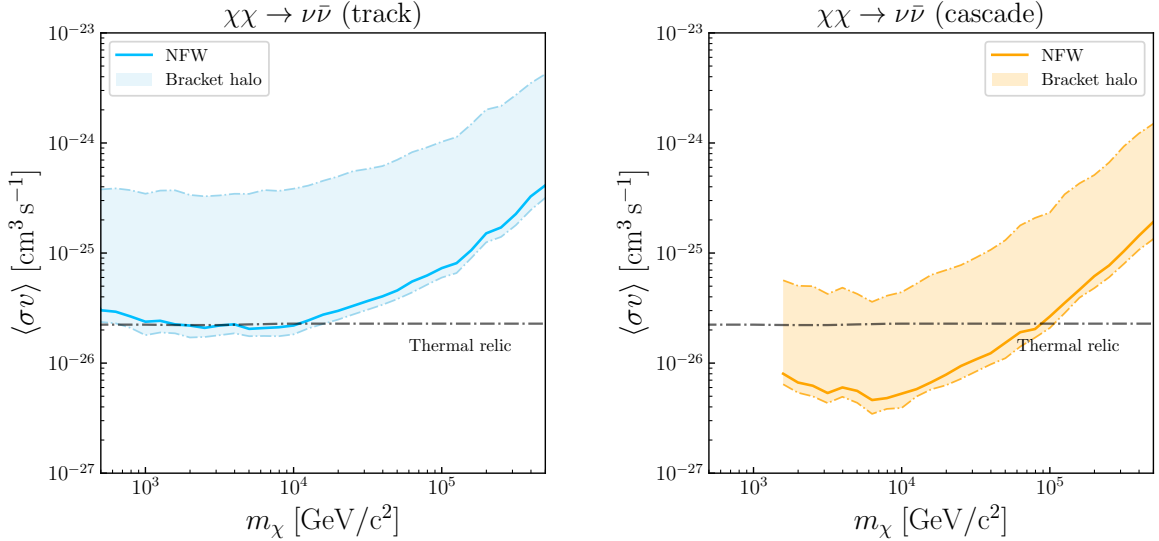


Figure 7: The expected sensitivity of the $\chi\chi \rightarrow \nu\bar{\nu}$ channel for both track (left) and cascade (right) events as in Fig. 4 but showing the effects from variations in the halo model. The solid curves indicate the limits using the NFW profile as a benchmark, while the coloured bands represent the variations from the Bracket halo model.

5 Particle Model Inference and Complementarity

In the previous sections, we demonstrated that the TRIDENT experiment can probe the DM thermal relic benchmark parameters under the assumption of a 100% annihilation rate into neutrinos. However, this is not a particularly likely scenario because neutrinos reside in left-handed SU(2) doublets, meaning many DM models with annihilations into neutrinos also have comparable annihilations into charged leptons and SM gauge bosons. The impact of TRIDENT's sensitivity depends on whether there exist well-motivated particle physics models that are not already excluded.

Although many models are available [63–68], we take as an example the $U(1)_{L_i-L_j}$ extension to the SM [69, 70]. This model is theoretically consistent, simple, and can accommodate DM. It was shown in Ref. [71] that high-energy neutrino telescopes would be able to provide particularly competitive limits [72]. This is primarily because the annihilation rate to neutrinos is relatively high, even when $m_\chi > 1$ TeV, an energy region where γ -ray telescopes lose sensitivity. Furthermore, the model does not couple to quarks at tree-level, weakening bounds from DM direct detection and colliders. Owing to TRIDENT's large exposure to the Galactic Centre and its excellent angular resolution, we expect it to provide leading sensitivity in this class of models. In this section we will show that TRIDENT expects to probe regions

of parameter space that are currently unconstrained, including the parameter regions that correspond to thermal freeze-out DM.

Before we describe the specifics of the particle model, we briefly review how we calculate the relevant DM properties used later. First, when calculating the thermally averaged cross-section during thermal freeze-out, we use [4, 73]

$$\langle \sigma v \rangle = \frac{2\pi^2 T}{(4\pi m_\chi^2 T K_2(m_\chi/T))^2} \int_{4m_\chi}^\infty ds \sqrt{s} (s - 4m_\chi^2) K_1\left(\frac{\sqrt{s}}{T}\right) \sigma_{\chi\chi \rightarrow ff}(s), \quad (5.1)$$

assuming the Maxwell-Boltzmann distribution of the DM phase space. Here, s is the Mandelstam variable, K_1 and K_2 are the modified Bessel function of the second kind, T is the temperature, which at freeze-out, we determine according to Ref. [5]. The cross-section $\sigma_{\chi\chi \rightarrow ff}$ is the total annihilation cross-section.

To calculate $\langle \sigma v \rangle$ in the astrophysical environments, one replaces the phase space distributions in Eq. (5.1) with the DM velocity distribution. Properly normalized, one can perform the following rearrangement [74, 75]

$$\langle \sigma v \rangle_i = \int dv_{\text{rel}} \tilde{f}_{\text{rel}}(v_{\text{rel}}) \sigma_i v_{\text{rel}}, \quad (5.2)$$

where v_{rel} is the relative DM velocity, and the subscript of σ signifies a specific annihilation channel. The velocity distribution function can be simplified if one assumes the Maxwell-Boltzmann distribution,

$$\tilde{f}_{\text{rel}}(v_{\text{rel}}) \equiv 4\pi v_{\text{rel}}^2 \int d^3 v_{\text{CM}} f(\mathbf{v}_{\text{CM}} + \mathbf{v}_{\text{rel}}/2) f(\mathbf{v}_{\text{CM}} - \mathbf{v}_{\text{rel}}/2) = \sqrt{\frac{2}{\pi}} \frac{v_{\text{rel}}^2}{v_0^3} \exp\left(-\frac{v_{\text{rel}}^2}{2v_0^2}\right), \quad (5.3)$$

where v_0 as the most probable velocity, which we take to be 220 km s^{-1} [76–78] for the Galactic Centre and 10 km s^{-1} [79, 80] for dwarf spheroidal galaxies. To map the indirect limits for a set of given annihilation channels, σ_i^{UL} , onto our model parameter space we determine the combined upper limit using model branching ratios Br_i ,

$$\langle \sigma v \rangle_{\text{tot}}^{\text{lim}} = \left(\sum_i \frac{\text{Br}_i}{\langle \sigma v \rangle_i^{\text{lim}}} \right)^{-1} \quad \text{where} \quad \text{Br}_i = \frac{\langle \sigma(\chi\bar{\chi} \rightarrow i) v \rangle}{\langle \sigma_{\text{tot}} v \rangle}. \quad (5.4)$$

We will show our TRIDENT projection as a combination of the track and cascade analysis above. For γ -ray telescopes, the most constraining bounds above $\sim 200 \text{ GeV}$ come from the H.E.S.S. Galactic Centre analysis [81]. As shown in Section 4.4, the Galactic Centre is subject to a large uncertainty due to the DM halo. Since the H.E.S.S. results for the relevant annihilation channels assume an Einasto profile [81], we estimate the H.E.S.S. NFW limit by rescaling according to the relative W^+W^- sensitivities assuming the Einasto and NFW profiles, respectively.

Finally we will also make use of the latest results from direct DM detection experiments. We will explicitly show the PandaX-4T result [82], but other xenon-based experiments such as LZ [83] and XENONnT [84] have achieved similar levels of sensitivity.

5.1 The $L_i - L_j$ Model

The $U(1)_{L_i - L_j}$ extension of the SM is one of the simplest theoretically consistent extensions available. There is the new $U(1)_{L_i - L_j}$ boson, Z' , which couples to the SM via the following current

$$j_\alpha^{L_i - L_j} = \bar{L}_i \gamma_\alpha L_i + \bar{\ell}_i \gamma_\alpha \ell_i - \bar{L}_j \gamma_\alpha L_j - \bar{\ell}_j \gamma_\alpha \ell_j, \quad (5.5)$$

where L and ℓ are the left-handed and right-handed lepton fields, respectively, the subscript denotes the flavour and $i \neq j$. For a DM candidate we introduce a Dirac DM particle, χ , which must interact with Z' in a vector-like way to maintain anomaly freedom [69, 70, 85–87]. The dark sector current is then

$$j_\alpha^\chi = \bar{\chi} \gamma_\alpha \chi = \bar{\chi}_L \gamma_\alpha \chi_L + \bar{\chi}_R \gamma_\alpha \chi_R, \quad (5.6)$$

such that the interaction terms are

$$\mathcal{L}_{\text{int}} = \frac{\epsilon}{2 \cos \theta_W} B_{\alpha\beta} Z'^{\alpha\beta} + g_{Z'}^{\text{DM}} Z'^\alpha j_\alpha^\chi + g_{Z'}^{\text{SM}} Z'^\alpha j_\alpha^{L_i - L_j},$$

where the $B_{\alpha\beta}$ is the SM hypercharge field strength tensor and θ_W is the weak mixing angle. We have also introduced couplings for the kinetic mixing, ϵ [88, 89], and the DM and SM currents, $g_{Z'}^{\text{DM}}$ and $g_{Z'}^{\text{SM}}$ respectively. We have normalised the kinetic mixing such that in the electroweak broken phase, ϵ can be determined by loop mixing between the photon and the new boson Z' [90, 91],

$$\epsilon(p \rightarrow 0) = \frac{e g_{Z'}^{\text{SM}}}{6\pi^2} \ln \left(\frac{m_j}{m_i} \right) \quad (5.7)$$

where e is the electric charge. Depending on the model flavour, the size of the kinetic mixing will vary slightly, for $L_e - L_\mu$, $L_e - L_\tau$, $L_\mu - L_\tau$, we have $\epsilon \sim g_{Z'}^{\text{SM}}/30$, $\epsilon \sim g_{Z'}^{\text{SM}}/20$, and $\epsilon \sim g_{Z'}^{\text{SM}}/60$ respectively. In the figures below, we show the results for the $L_\mu - L_\tau$ model and comment on the differences for the other $L_i - L_j$ models.

When $m_{Z'} > m_\chi$, DM annihilation proceeds through s-channel scattering into charged leptons and neutrinos with a branching ratio of $\sim 2/3$ and $\sim 1/3$, respectively. When $m_\chi > m_{Z'}$, the $\chi\bar{\chi} \rightarrow Z'Z'$ annihilation opens up and can be important. For a neutrino telescope this process will be detectable via the decay particles from the Z' , leading to the box-shaped 4ν spectra described in Section 2, the projected TRIDENT sensitivities to which were shown in Fig. 4. For such channels we determine the branching ratio by

$$\text{Br}_{i\bar{i} j\bar{j}} = \text{Br}_{Z'Z'} \times \left(\frac{\Gamma(Z' \rightarrow i\bar{i})}{\Gamma_{\text{tot}}} \right) \times \left(\frac{\Gamma(Z' \rightarrow j\bar{j})}{\Gamma_{\text{tot}}} \right), \quad (5.8)$$

where we multiply by 2 if $i \neq j$. For the $\chi\bar{\chi} \rightarrow Z'Z' \rightarrow \nu\bar{\nu}\ell^+\ell^-$ channel, we estimate the sensitivity by rescaling the 4ν sensitivity by a factor of 2 to reflect the reduced signal spectra dN_ν/dE_ν .

We show our projected TRIDENT limit on the parameter space in the left panel of Fig. 8 in red, assuming $g_{Z'}^{\text{DM}} = g_{Z'}^{\text{SM}} = 1.0$ and an NFW DM profile. One can see that the TRIDENT sensitivity will be able to cover regions close to or over the thermal relic line. When $m_{Z'} < m_\chi$ the t-channel $\chi\bar{\chi} \rightarrow Z'Z'$ process can become important, $\text{Br}_{Z'Z'} \sim 0.25$ of the total annihilation cross-section. In the same regions of parameter space, the relatively light Z' compared to χ can contribute to a Sommerfeld enhancement. This enhancement arises from non-relativistic multiple exchanges of the light mediator, which increase the annihilation

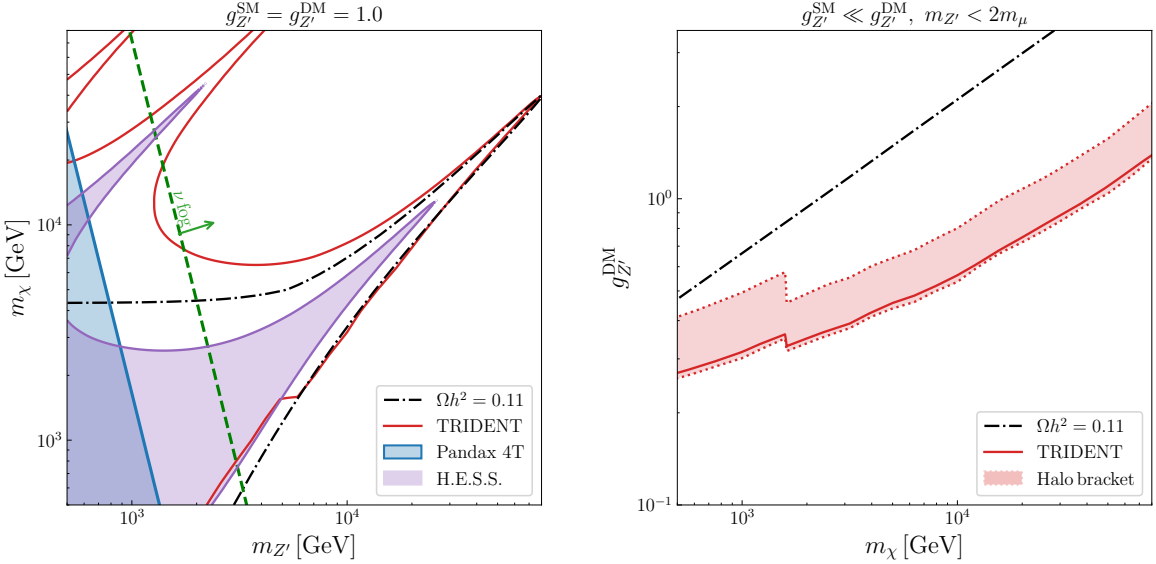


Figure 8: Plots showing the reach of TRIDENT on the model we consider here. Left panel shows the $(m_{Z'}, m_\chi)$ plane assuming $g_{Z'}^{\text{SM}} = g_{Z'}^{\text{DM}} = 1.0$. We show the strongest limits from γ -ray telescopes (H.E.S.S. [81]) and direct detection (PandaX-4T [82]) with the purple and blue shaded regions, respectively. The neutrino fog [103] is shown by the green dashed line. Right panel shows the TRIDENT sensitivity in the $(m_\chi, g_{Z'}^{\text{DM}})$ plane, now assuming $g_{Z'}^{\text{SM}} \ll g_{Z'}^{\text{DM}}$. In both panels we show the calculated relic line cast from Ref. [5].

rate at low velocities [92, 93]. We use the analytic approximation given in Refs. [94–96]. Due to both the t-channel and Sommerfeld enhancement, it is not trivial to see exactly how the limits vary for different couplings. When the s-channel annihilation dominates, $\langle\sigma v\rangle \sim (g_{Z'}^{\text{SM}} g_{Z'}^{\text{DM}})^2 / (4m_\chi^2 - m_{Z'}^2)^2$, and smaller couplings simply require smaller masses accordingly.

In addition to the TRIDENT projections we show the constraints on this model from the most sensitive indirect and direct detection results in shaded purple and blue, respectively. The charged lepton decays, $\tau^+\tau^-$ and $\mu^+\mu^-$ occurring at tree-level dominate the γ -ray limits for this model [81]. Whereas the direct detection signal is produced only via the loop induced kinetic mixing, Eq. (5.7). To determine the elastic nucleon cross-section, we follow Refs. [97–101] and determine that when $m_{Z'} > 500$ GeV, the DM-neutron cross-section is zero at first order and the DM-proton cross-section can be written as

$$\sigma_{\chi p} = \frac{m_\chi^2 m_p^2}{\pi(m_\chi + m_p)^2} \frac{e^2 (g_{Z'}^{\text{DM}})^2 \epsilon^2}{m_{Z'}^4}. \quad (5.9)$$

Furthermore, we also show by way of a green dashed line, where the irreducible neutrino background from coherent elastic neutrino-nucleus scattering will come into effect [102, 103]. At these energies the dominant neutrino source is atmospheric neutrinos which will be indistinguishable from a DM particle with mass above ~ 50 GeV. We can see that the TRIDENT sensitivities calculated in this work reach deep into the neutrino floor.

For the thermal relic and the TRIDENT constraint, the lines in the left panel of Fig. 8 would be unchanged for the $L_e - L_\mu$ and $L_e - L_\tau$ models. However, the PandaX and neutrino floor lines would move a little to the right due to a slight increase in the kinetic mixing. For the H.E.S.S. constraint, a slight weakening of the limit would occur for the $L_e - L_\mu$ model

because the e^+e^- and $\mu^+\mu^-$ final-states are less constrained with respect to $\tau^+\tau^-$.

In the right panel of Fig. 8 we focus on the scenario where neutrino telescopes give the only constraints. This is the secluded $U(1)_{L_\mu-L_\tau}$ model and occurs when the Z' mediator is very light, and $g_{Z'}^{\text{DM}} \gg g_{Z'}^{\text{SM}}$ [104]. In this case the relic abundance can still be achieved via a dark sector freeze-out. The most interesting possibility for TRIDENT is when $m_{Z'} < 2m_\mu$ which results in $\text{Br}_{4\nu} \approx 1$. For such a light boson, current constraints require $g_{Z'}^{\text{SM}} \lesssim 4 \times 10^{-4}$ [105–108] and $m_{Z'} \gtrsim 5 \text{ MeV}$ [109].

For the entire range of m_χ in the right panel of Fig. 8 the Sommerfeld enhancement is in effect, allowing our predicted sensitivity to overcome the uncertainty on the DM halo. The solid red line is for the NFW profile and the red shaded region brackets the uncertainty in the halo as described in Section 4.4. We see that when $m_\chi \gtrsim 600 \text{ GeV}$, TRIDENT’s sensitivities will be able to confidently exclude this scenario for thermally produced DM.

We quickly comment on other proposed experimental tests for this model, many of which are reviewed in Ref. [72]. The key limitation for collider searches is the achieved centre-of-mass energies, the largest of which is the LHC, but since our model does not couple to quarks at tree-level, most limits are not relevant. In fact, measurements at LEP-II remain the most stringent, $m_{Z'} \gtrsim 209 \text{ GeV}$ [110, 111], this underscores the power a future lepton collider could have on this model [112–114].

6 Summary and Outlook

In this paper we have presented the first DM annihilation sensitivity forecasts for TRIDENT. This is an important step for establishing the analysis framework and can be used to inform any pre-deployment optimization. Our results show that cascade events will bring substantial improvements to the DM sensitivity, by over a factor of 2 compared to a track-only analysis. In fact, the cascade sensitivity result shows that TRIDENT will be able to probe the thermal relic cross-section values for DM masses between $10^3 - 10^5 \text{ GeV}$. We obtain sensitivities down to $\langle \sigma v \rangle \approx 5 \times 10^{-27} \text{ cm}^3 \text{ s}^{-1}$ at $m_\chi = 10 \text{ TeV}$. This area of parameter space is still untested and is one of the last regions for the ‘WIMP miracle’.

As always with indirect detection, one has to contend with uncertainties in the DM distribution, which will weaken TRIDENT’s sensitivity. Additionally, the background flux of neutrinos originating from the interactions of hadronic cosmic rays and interstellar gas remains largely unknown and can limit the sensitivity further. We estimate the effect this background will have on neutrino telescopes’ search for DM annihilation signals from the Galactic Centre. We believe that this is the first time such a background has been incorporated and we find that its impact is greater at energies above $\sim 10 \text{ TeV}$ where at most the sensitivities are weakened by a factor of ~ 2 . We also highlight the possibility that this background could mimic a DM signal, motivating further research and the development of analysis techniques that distinguish between the two signals.

In order to emphasise the future impact of TRIDENT we contextualize our model-independent limits with a specific particle physics model, the $U(1)_{L_i-L_j}$, which represents a more realistic scenario than 100% annihilations into neutrinos. We demonstrate that TRIDENT remains sensitive to parameter values consistent with a thermal relic, as annihilations into neutrinos are still substantial. At energies above 1 TeV , γ -ray telescopes and direct dark matter detection searches lose sensitivity, opening a complementary discovery for neutrino telescopes. Due to its large exposure to the Galactic Centre and excellent angular resolution,

TRIDENT is uniquely positioned to exploit this window. For example, when $m_{Z'}$ and m_χ are both at ~ 10 TeV scale, TRIDENT will probe deep into the ‘neutrino fog’, where direct detection experiments will struggle to penetrate. There remain substantial regions where both direct and indirect detection experiments complement each other and would provide independent verification of any signal, which may be needed given the Galactic plane neutrino background. The accompanying γ -ray signals predicted by the model will also be a source of complementarity aiding both background and particle model discrimination. Furthermore, since relic DM above 1 TeV requires resonances or leads to Sommerfeld enhancements, the velocity distribution in the DM profile could be more important than usually assumed for velocity independent annihilation. The TRIDENT sensitivity we report here motivates a more careful analysis.

Acknowledgments

The authors would like to thank the following individuals for their helpful comments and discussions: C. Arina, P. Foldenauer, S. Hernández Cadena, X. G. He, X. G. Lu, S. K. Mondal, K. Ng, H. B. Shao, S. H. Hao, and T. L. Zhu. S. Kaci acknowledges the support of G. Giacinti, funded by the National Natural Science Foundation of China under Grants Nos. 12350610239, and 12393853. A. Cheek acknowledges the support of S. Ge, funded by the National Natural Science Foundation of China (Grant Nos. 12425506, 12375101, 12090060, and 12090064) and the Double First-Class startup funds by Shanghai Jiao Tong University. X. Xiang would like to thank the Double First-Class startup funds by Shanghai Jiao Tong University. I. Morton-Blake also acknowledges the National Natural Science Foundation of China Grant No. 12350410499 and the Kuan-Cheng Wang Education Foundation.

References

- [1] G. Bertone and D. Hooper, *History of dark matter*, *Rev. Mod. Phys.* **90** (2018) 045002 [[1605.04909](#)].
- [2] M. Cirelli, A. Strumia and J. Zupan, *Dark Matter*, [2406.01705](#).
- [3] R.J. Scherrer and M.S. Turner, *On the Relic, Cosmic Abundance of Stable Weakly Interacting Massive Particles*, *Phys. Rev. D* **33** (1986) 1585.
- [4] P. Gondolo and G. Gelmini, *Cosmic abundances of stable particles: Improved analysis*, *Nucl. Phys. B* **360** (1991) 145.
- [5] G. Steigman, B. Dasgupta and J.F. Beacom, *Precise Relic WIMP Abundance and its Impact on Searches for Dark Matter Annihilation*, *Phys. Rev. D* **86** (2012) 023506 [[1204.3622](#)].
- [6] K. Griest and M. Kamionkowski, *Unitarity Limits on the Mass and Radius of Dark Matter Particles*, *Phys. Rev. Lett.* **64** (1990) 615.
- [7] J.E. Gunn, B.W. Lee, I. Lerche, D.N. Schramm and G. Steigman, *Some Astrophysical Consequences of the Existence of a Heavy Stable Neutral Lepton*, *Astrophys. J.* **223** (1978) 1015.
- [8] F.W. Stecker, *The Cosmic Gamma-Ray Background from the Annihilation of Primordial Stable Neutral Heavy Leptons*, *Astrophys. J.* **223** (1978) 1032.
- [9] Y.B. Zeldovich, A.A. Klypin, M.Y. Khlopov and V.M. Chechetkin, *Astrophysical constraints on the mass of heavy stable neutral leptons*, *Sov. J. Nucl. Phys.* **31** (1980) 664.
- [10] D. Hooper and L. Goodenough, *Dark Matter Annihilation in The Galactic Center As Seen by the Fermi Gamma Ray Space Telescope*, *Phys. Lett. B* **697** (2011) 412 [[1010.2752](#)].

[11] FERMI-LAT collaboration, *The Fermi Galactic Center GeV Excess and Implications for Dark Matter*, *Astrophys. J.* **840** (2017) 43 [[1704.03910](#)].

[12] FERMI-LAT collaboration, *Searching for Dark Matter Annihilation from Milky Way Dwarf Spheroidal Galaxies with Six Years of Fermi Large Area Telescope Data*, *Phys. Rev. Lett.* **115** (2015) 231301 [[1503.02641](#)].

[13] AMS collaboration, *The Alpha Magnetic Spectrometer (AMS) on the international space station: Part II — Results from the first seven years*, *Phys. Rept.* **894** (2021) 1.

[14] R.K. Leane, T.R. Slatyer, J.F. Beacom and K.C.Y. Ng, *GeV-scale thermal WIMPs: Not even slightly ruled out*, *Phys. Rev. D* **98** (2018) 023016 [[1805.10305](#)].

[15] HAWC collaboration, *Dark Matter Limits From Dwarf Spheroidal Galaxies with The HAWC Gamma-Ray Observatory*, *Astrophys. J.* **853** (2018) 154 [[1706.01277](#)].

[16] HESS collaboration, *Searches for gamma-ray lines and 'pure WIMP' spectra from Dark Matter annihilations in dwarf galaxies with H.E.S.S.*, *JCAP* **11** (2018) 037 [[1810.00995](#)].

[17] CTA collaboration, *Sensitivity of the Cherenkov Telescope Array to a dark matter signal from the Galactic centre*, *JCAP* **01** (2021) 057 [[2007.16129](#)].

[18] LHAASO collaboration, *Constraints on Ultraheavy Dark Matter Properties from Dwarf Spheroidal Galaxies with LHAASO Observations*, *Phys. Rev. Lett.* **133** (2024) 061001 [[2406.08698](#)].

[19] ANTARES collaboration, *Search of Dark Matter Annihilation in the Galactic Centre using the ANTARES Neutrino Telescope*, *JCAP* **10** (2015) 068 [[1505.04866](#)].

[20] C.A. Argüelles, A. Diaz, A. Kheirandish, A. Olivares-Del-Campo, I. Safa and A.C. Vincent, *Dark matter annihilation to neutrinos*, *Rev. Mod. Phys.* **93** (2021) 035007 [[1912.09486](#)].

[21] A. Ishihara, *The next generation neutrino telescope: Icecube-gen2*, in *Proc. 38th Int. Cosmic Ray Conf. (ICRC2023)*, 2023, DOI [[2308.09427](#)].

[22] KM3NET collaboration, *First searches for dark matter with the KM3NeT neutrino telescopes*, *JCAP* **03** (2025) 058 [[2411.10092](#)].

[23] L.S. Miranda, S. Basegmez du Pree, K.C.Y. Ng, A. Cheek and C. Arina, *Towards detecting super-GeV dark matter via annihilation to neutrinos*, *JCAP* **08** (2023) 006 [[2211.12235](#)].

[24] R. Abbasi, M. Ackermann, J. Adams, J.A. Aguilar, M. Ahlers, M. Ahrens et al., *Observation of high-energy neutrinos from the galactic plane*, *Science* **380** (2023) 1338.

[25] A. Ibarra, S. Lopez Gehler and M. Pato, *Dark matter constraints from box-shaped gamma-ray features*, *JCAP* **07** (2012) 043 [[1205.0007](#)].

[26] C. Garcia-Cely and J. Heeck, *Indirect searches of dark matter via polynomial spectral features*, *JCAP* **08** (2016) 023 [[1605.08049](#)].

[27] Q. Liu, J. Lazar, C.A. Argüelles and A. Kheirandish, *χ arov: a tool for neutrino flux generation from WIMPs*, *JCAP* **10** (2020) 043 [[2007.15010](#)].

[28] C.W. Bauer, N.L. Rodd and B.R. Webber, *Dark matter spectra from the electroweak to the Planck scale*, *JHEP* **06** (2021) 121 [[2007.15001](#)].

[29] C. Arina, M. Di Mauro, N. Fornengo, J. Heisig, A. Jueid and R.R. de Austri, *CosmiXs: cosmic messenger spectra for indirect dark matter searches*, *JCAP* **03** (2024) 035 [[2312.01153](#)].

[30] I. Esteban, M.C. Gonzalez-Garcia, M. Maltoni, I. Martinez-Soler, J.P. Pinheiro and T. Schwetz, *Nufit-6.0: updated global analysis of three-flavor neutrino oscillations*, *Journal of High Energy Physics* **2024** (2025) 1.

[31] J.F. Navarro, C.S. Frenk and S.D.M. White, *The Structure of cold dark matter halos*, *Astrophys. J.* **462** (1996) 563 [[astro-ph/9508025](#)].

[32] Y. Sofue, *Rotation curve of the milky way and the dark matter density*, *Galaxies* **8** (2020) 37.

[33] H. Shao, F. Zhang, Q. Chang, S. Hao, R. Cao, J. Huang et al., *A Cost Effective Optimization of the hybrid-DOM Design for TRIDENT*, [2507.10256](#).

[34] I. Morton-Blake, F. Zhang, Q. Chang, S. Hao, W. Huang, W. Tian et al., *Optimising underwater neutrino telescopes for all-flavour point source sensitivity*, *arXiv e-prints* (2025) [[2510.24395](#)].

[35] C. Bierlich, S. Chakraborty, N. Desai, L. Gellersen, I. Helenius, P. Ilten et al., *A comprehensive guide to the physics and usage of PYTHIA 8.3*, *SciPost Phys. Codebases* (2022) 8.

[36] R. Ulrich, T. Pierog and C. Baus, *Cosmic ray monte carlo package, crmc*, *Zenodo, Aug* **10** (2021) .

[37] G. Collaboration, S. Agostinelli et al., *Geant4—a simulation toolkit*, *Nucl. Instrum. Meth. A* **506** (2003) 0.

[38] S. Blyth, *Opticks: Gpu optical photon simulation for particle physics using nvidia® optixtm*, in *EPJ Web of Conferences*, vol. 214, p. 02027, EDP Sciences, 2019.

[39] Z.P. Ye, F. Hu, G.J. Zhuang et al., *A multi-cubic-kilometre neutrino telescope in the western Pacific Ocean*, *Nature Astronomy* **7** (2023) 1241–1249.

[40] S. Aiello, A. Albert, A. Alhebsi, M. Alshamsi, S.A. Garre, A. Ambrosone et al., *First searches for dark matter with the km3net neutrino telescopes*, *Journal of Cosmology and Astroparticle Physics* **2025** (2025) 058.

[41] J.P. Yañez and A. Fedynitch, *Data-driven muon-calibrated neutrino flux*, *Physical Review D* **107** (2023) 123037.

[42] R. Abbasi, M. Ackermann, J. Adams, J. Aguilar, M. Ahlers, M. Ahrens et al., *Improved characterization of the astrophysical muon–neutrino flux with 9.5 years of icecube data*, *The Astrophysical Journal* **928** (2022) 50.

[43] S.S. Wilks, *The large-sample distribution of the likelihood ratio for testing composite hypotheses*, *The annals of mathematical statistics* **9** (1938) 60.

[44] S. Kaci and G. Giacinti, *Imprints of pev cosmic-ray sources on the diffuse gamma-ray emission*, *Journal of Cosmology and Astroparticle Physics* **2025** (2025) 049.

[45] S. Kaci, G. Giacinti, F. Aharonian and J.-S. Wang, *Microquasars as the major contributors to galactic cosmic rays around the "knee"*, 2025.

[46] F. Zhang, S. Kaci, G. Giacinti, I. Morton-Blake and D. Xu, *Probing the galactic neutrino emission with trident*, In prep. (2025).

[47] P. Mertsch and A. Vittino, *Bayesian inference of three-dimensional gas maps: I. Galactic CO*, [2012.15770](#).

[48] P. Mertsch and V.H.M. Phan, *Bayesian inference of three-dimensional gas maps - II. Galactic HI*, *Astron. Astrophys.* **671** (2023) A54 [[2202.02341](#)].

[49] A.W. Strong and I.V. Moskalenko, *Propagation of cosmic-ray nucleons in the galaxy*, *The Astrophysical Journal* **509** (1998) 212.

[50] C. Evoli, D. Gaggero, D. Grasso and L. Maccione, *Cosmic ray nuclei, antiprotons and gamma rays in the galaxy: a new diffusion model*, *Journal of Cosmology and Astroparticle Physics* **2008** (2008) 018.

[51] C. Evoli, D. Gaggero, A. Vittino, G.D. Bernardo, M.D. Mauro, A. Ligorini et al., *Cosmic-ray propagation with dragon2: I. numerical solver and astrophysical ingredients*, *Journal of Cosmology and Astroparticle Physics* **2017** (2017) 015.

[52] A. Vallenari, A.G. Brown, T. Prusti, J.H. De Bruijne, F. Arenou, C. Babusiaux et al., *Gaia data release 3-summary of the content and survey properties*, *Astronomy & Astrophysics* **674** (2023) A1.

[53] R.J.J. Grand, F. Fragkoudi, F.A. Gómez, A. Jenkins, F. Marinacci, R. Pakmor et al., *Overview and public data release of the augmented Auriga Project: cosmological simulations of dwarf and Milky Way-mass galaxies*, *Mon. Not. Roy. Astron. Soc.* **532** (2024) 1814 [[2401.08750](#)].

[54] A. Wetzel et al., *Public Data Release of the FIRE-2 Cosmological Zoom-in Simulations of Galaxy Formation*, *Astrophys. J. Suppl.* **265** (2023) 44 [[2202.06969](#)].

[55] M.P. Rey, O. Agertz, T.K. Starkenburg, F. Renaud, G.D. Joshi, A. Pontzen et al., *VINTERGATAN-GM: The cosmological imprints of early mergers on Milky-Way-mass galaxies*, *Mon. Not. Roy. Astron. Soc.* **521** (2023) 995 [[2211.15689](#)].

[56] A. Pillepich et al., *First results from the TNG50 simulation: the evolution of stellar and gaseous discs across cosmic time*, *Mon. Not. Roy. Astron. Soc.* **490** (2019) 3196 [[1902.05553](#)].

[57] Gaia Collaboration, A.G.A. Brown, A. Vallenari et al., *Gaia data release 1. summary of the astrometric, photometric, and survey properties*, *Astronomy & Astrophysics* **595** (2016) A2.

[58] Gaia Collaboration, A.G.A. Brown, A. Vallenari et al., *Gaia data release 2. summary of the contents and survey properties*, *Astronomy & Astrophysics* **616** (2018) A1.

[59] Gaia Collaboration, A.G.A. Brown, A. Vallenari et al., *Gaia early data release 3. summary of the contents and survey properties*, *Astronomy & Astrophysics* **649** (2021) A1.

[60] Y. Zhou, X. Li, Y. Huang and H. Zhang, *The Circular Velocity Curve of the Milky Way from 5–25 kpc Using Luminous Red Giant Branch Stars*, *Astrophys. J.* **946** (2023) 73 [[2212.10393](#)].

[61] X. Ou, A.-C. Eilers, L. Necib and A. Frebel, *The dark matter profile of the milky way inferred from its circular velocity curve*, *Monthly Notices of the Royal Astronomical Society* **528** (2024) 693.

[62] A. Hussein, L. Necib, M. Kaplinghat, S.Y. Kim, A. Wetzel, J.I. Read et al., *Theoretical Predictions for the Inner Dark Matter Distribution in the Milky Way Informed by Simulations*, [2501.14868](#).

[63] C. El Aisati, C. Garcia-Cely, T. Hambye and L. Vanderheyden, *Prospects for discovering a neutrino line induced by dark matter annihilation*, *JCAP* **10** (2017) 021 [[1706.06600](#)].

[64] M. Blennow, E. Fernandez-Martinez, A. Olivares-Del Campo, S. Pascoli, S. Rosauro-Alcaraz and A.V. Titov, *Neutrino Portals to Dark Matter*, *Eur. Phys. J. C* **79** (2019) 555 [[1903.00006](#)].

[65] J. Kopp, L. Michaels and J. Smirnov, *Loopy Constraints on Leptophilic Dark Matter and Internal Bremsstrahlung*, *JCAP* **04** (2014) 022 [[1401.6457](#)].

[66] A. Ibarra and S. Wild, *Dirac dark matter with a charged mediator: a comprehensive one-loop analysis of the direct detection phenomenology*, *JCAP* **05** (2015) 047 [[1503.03382](#)].

[67] C. Arina, B. Fuks and L. Mantani, *A universal framework for t-channel dark matter models*, *Eur. Phys. J. C* **80** (2020) 409 [[2001.05024](#)].

[68] C. Arina et al., *t-channel dark matter models – a whitepaper*, *Eur. Phys. J. C* **85** (2025) 975 [[2504.10597](#)].

[69] X.-G. He, G.C. Joshi, H. Lew and R.R. Volkas, *Simplest Z-prime model*, *Phys. Rev. D* **44** (1991) 2118.

[70] X.G. He, G.C. Joshi, H. Lew and R.R. Volkas, *NEW Z-prime PHENOMENOLOGY*, *Phys. Rev. D* **43** (1991) 22.

[71] S. Basegmez Du Pree, C. Arina, A. Cheek, A. Dekker, M. Chianese and S. Ando, *Robust Limits from Upcoming Neutrino Telescopes and Implications on Minimal Dark Matter Models*, *JCAP* **05** (2021) 054 [[2103.01237](#)].

[72] N. Bernal, J.P. Neto, J. Silva-Malpartida and F.S. Queiroz, *Enabling thermal dark matter within the vanilla $L\mu$ - $L\tau$ model*, *Phys. Rev. D* **112** (2025) 075042 [[2507.02048](#)].

[73] M. Bauer and T. Plehn, *Yet Another Introduction to Dark Matter: The Particle Physics Approach*, vol. 959 of *Lecture Notes in Physics*, Springer (2019), [10.1007/978-3-030-16234-4](#), [[1705.01987](#)].

[74] F. Ferrer and D.R. Hunter, *The impact of the phase-space density on the indirect detection of dark matter*, *JCAP* **09** (2013) 005 [[1306.6586](#)].

[75] F. Ambrogi, C. Arina, M. Backovic, J. Heisig, F. Maltoni, L. Mantani et al., *MadDM v.3.0: a Comprehensive Tool for Dark Matter Studies*, *Phys. Dark Univ.* **24** (2019) 100249 [[1804.00044](#)].

[76] Y.-Y. Mao, L.E. Strigari, R.H. Wechsler, H.-Y. Wu and O. Hahn, *Halo-to-halo similarity and scatter in the velocity distribution of dark matter*, *The Astrophysical Journal* **764** (2013) 35.

[77] P.J. McMillan, *The mass distribution and gravitational potential of the Milky Way*, *Mon. Not. Roy. Astron. Soc.* **465** (2016) 76 [[1608.00971](#)].

[78] N. Bozorgnia and G. Bertone, *Implications of hydrodynamical simulations for the interpretation of direct dark matter searches*, *Int. J. Mod. Phys. A* **32** (2017) 1730016 [[1705.05853](#)].

[79] M.G. Walker, M. Mateo, E.W. Olszewski, O.Y. Gnedin, X. Wang, B. Sen et al., *Velocity dispersion profiles of seven dwarf spheroidal galaxies*, *The Astrophysical Journal* **667** (2007) L53–L56.

[80] M.G. Walker, *Dark Matter in the Milky Way’s Dwarf Spheroidal Satellites*, [1205.0311](#).

[81] H.E.S.S. collaboration, *Search for Dark Matter Annihilation Signals in the H.E.S.S. Inner Galaxy Survey*, *Phys. Rev. Lett.* **129** (2022) 111101 [[2207.10471](#)].

[82] PANDAX collaboration, *Dark Matter Search Results from 1.54 Tonne-Year Exposure of PandaX-4T*, *Phys. Rev. Lett.* **134** (2025) 011805 [[2408.00664](#)].

[83] LZ collaboration, *Constraints on Covariant Dark-Matter–Nucleon Effective Field Theory Interactions from the First Science Run of the LUX-ZEPLIN Experiment*, *Phys. Rev. Lett.* **133** (2024) 221801 [[2404.17666](#)].

[84] XENON collaboration, *WIMP Dark Matter Search Using a 3.1 Tonne-Year Exposure of the XENONnT Experiment*, *Phys. Rev. Lett.* **135** (2025) 221003 [[2502.18005](#)].

[85] S.M. Barr, B. Bednarz and C. Benesh, *Anomaly Constraints and New $U(1)$ Gauge Bosons*, *Phys. Rev. D* **34** (1986) 235.

[86] J.A. Dror, R. Lasenby and M. Pospelov, *New constraints on light vectors coupled to anomalous currents*, *Phys. Rev. Lett.* **119** (2017) 141803 [[1705.06726](#)].

[87] J. Ellis, M. Fairbairn and P. Tunney, *Anomaly-Free Dark Matter Models are not so Simple*, *JHEP* **08** (2017) 053 [[1704.03850](#)].

[88] L.B. Okun, *LIMITS OF ELECTRODYNAMICS: PARAPHOTONS?*, *Sov. Phys. JETP* **56** (1982) 502.

[89] B. Holdom, *Two $U(1)$ ’s and Epsilon Charge Shifts*, *Phys. Lett. B* **166** (1986) 196.

[90] T. Araki, S. Hoshino, T. Ota, J. Sato and T. Shimomura, *Detecting the $L_\mu - L_\tau$ gauge boson at Belle II*, *Phys. Rev. D* **95** (2017) 055006 [[1702.01497](#)].

[91] M. Bauer and P. Foldenauer, *Consistent Theory of Kinetic Mixing and the Higgs Low-Energy Theorem*, *Phys. Rev. Lett.* **129** (2022) 171801 [[2207.00023](#)].

[92] J. Hisano, S. Matsumoto, M. Nagai, O. Saito and M. Senami, *Non-perturbative effect on thermal relic abundance of dark matter*, *Phys. Lett. B* **646** (2007) 34 [[hep-ph/0610249](#)].

[93] M. Cirelli, A. Strumia and M. Tamburini, *Cosmology and Astrophysics of Minimal Dark Matter*, *Nucl. Phys. B* **787** (2007) 152 [[0706.4071](#)].

[94] T.R. Slatyer, *The Sommerfeld enhancement for dark matter with an excited state*, *JCAP* **02** (2010) 028 [[0910.5713](#)].

[95] J.L. Feng, M. Kaplinghat and H.-B. Yu, *Sommerfeld Enhancements for Thermal Relic Dark Matter*, *Phys. Rev. D* **82** (2010) 083525 [[1005.4678](#)].

[96] S. Cassel, *Sommerfeld factor for arbitrary partial wave processes*, *J. Phys. G* **37** (2010) 105009 [[0903.5307](#)].

[97] J.A. Evans, S. Gori and J. Shelton, *Looking for the WIMP Next Door*, *JHEP* **02** (2018) 100 [[1712.03974](#)].

[98] M. Bauer, P. Foldenauer and J. Jaeckel, *Hunting All the Hidden Photons*, *JHEP* **07** (2018) 094 [[1803.05466](#)].

[99] J.-X. Pan, M. He, X.-G. He and G. Li, *Scrutinizing a massless dark photon: basis independence*, *Nucl. Phys. B* **953** (2020) 114968 [[1807.11363](#)].

[100] P. Foldenauer, *Phenomenology of Extra Abelian Gauge Symmetries*, Ph.D. thesis, U. Heidelberg (main), 7, 2019. 10.11588/heidok.00026777.

[101] D. Alonso-González, D. Cerdeño, P. Foldenauer and J.M. No, *GeV-scale thermal dark matter from dark photons: tightly constrained, yet allowed*, [2507.11376](#).

[102] J. Billard, L. Strigari and E. Figueroa-Feliciano, *Implication of neutrino backgrounds on the reach of next generation dark matter direct detection experiments*, *Phys. Rev. D* **89** (2014) 023524 [[1307.5458](#)].

[103] C.A.J. O’Hare, *New definition of the neutrino floor for direct dark matter searches*, *Physical Review Letters* **127** (2021) .

[104] M. Pospelov, A. Ritz and M.B. Voloshin, *Secluded WIMP Dark Matter*, *Phys. Lett. B* **662** (2008) 53 [[0711.4866](#)].

[105] NA64 collaboration, *First Results in the Search for Dark Sectors at NA64 with the CERN SPS High Energy Muon Beam*, *Phys. Rev. Lett.* **132** (2024) 211803 [[2401.01708](#)].

[106] P. Foldenauer and J. Hoefken Zink, *How to rule out $(g-2)_\mu$ in $U(1)_{L_\mu-L_\tau}$ with white dwarf cooling*, *JHEP* **07** (2024) 096 [[2405.00094](#)].

[107] MUON G-2 collaboration, *Measurement of the Positive Muon Anomalous Magnetic Moment to 127 ppb*, *Phys. Rev. Lett.* **135** (2025) 101802 [[2506.03069](#)].

[108] M.-W. Li, X.-G. He, A. Cheek and X. Chu, *The $U(1)L_\mu-L_\tau$ model meets the new $(g-2)_\mu$ data and muon neutrino trident scattering*, *Phys. Lett. B* **871** (2025) 139949 [[2506.05511](#)].

[109] M. Escudero, D. Hooper, G. Krnjaic and M. Pierre, *Cosmology with A Very Light $L_\mu - L_\tau$ Gauge Boson*, *JHEP* **03** (2019) 071 [[1901.02010](#)].

[110] OPAL collaboration, *Tests of the standard model and constraints on new physics from measurements of fermion pair production at 189-GeV to 209-GeV at LEP*, *Eur. Phys. J. C* **33** (2004) 173 [[hep-ex/0309053](#)].

- [111] ALEPH collaboration, *Fermion pair production in e^+e^- collisions at 189-209-GeV and constraints on physics beyond the standard model*, *Eur. Phys. J. C* **49** (2007) 411 [[hep-ex/0609051](#)].
- [112] G.-y. Huang, F.S. Queiroz and W. Rodejohann, *Gauged $L_\mu - L_\tau$ at a muon collider*, *Phys. Rev. D* **103** (2021) 095005 [[2101.04956](#)].
- [113] INTERNATIONAL MUON COLLIDER collaboration, *The Muon Collider*, [2504.21417](#).
- [114] CEPC STUDY GROUP collaboration, *CEPC Conceptual Design Report: Volume 2 - Physics & Detector*, [1811.10545](#).